

## Finite size line broadening and superradiance of optical transitions in two dimensional long-range ordered molecular aggregates

Mathias Müller, Alexander Paulheim, Alexander Eisfeld, and Moritz Sokolowski

Citation: *J. Chem. Phys.* **139**, 044302 (2013); doi: 10.1063/1.4813521

View online: <http://dx.doi.org/10.1063/1.4813521>

View Table of Contents: <http://jcp.aip.org/resource/1/JCPSA6/v139/i4>

Published by the [AIP Publishing LLC](#).

---

### Additional information on *J. Chem. Phys.*

Journal Homepage: <http://jcp.aip.org/>

Journal Information: [http://jcp.aip.org/about/about\\_the\\_journal](http://jcp.aip.org/about/about_the_journal)

Top downloads: [http://jcp.aip.org/features/most\\_downloaded](http://jcp.aip.org/features/most_downloaded)

Information for Authors: <http://jcp.aip.org/authors>

## ADVERTISEMENT



Explore the **Most Cited**  
Collection in Applied Physics

**AIP**  
Publishing

# Finite size line broadening and superradiance of optical transitions in two dimensional long-range ordered molecular aggregates

Mathias Müller,<sup>1</sup> Alexander Paulheim,<sup>1</sup> Alexander Eisfeld,<sup>2</sup> and Moritz Sokolowski<sup>1,a)</sup>

<sup>1</sup>*Institut für Physikalische und Theoretische Chemie der Universität Bonn, Wegelerstrasse 12, 53115 Bonn, Germany*

<sup>2</sup>*Max-Planck-Institut für Physik komplexer Systeme, Nöthnitzer Straße 38, 01187 Dresden, Germany*

(Received 28 March 2013; accepted 26 June 2013; published online 22 July 2013)

The width and asymmetry of the line shape of the optical transition of a sample of two dimensional (2D) molecular J-aggregates was found to be related to a finite-size effect. The 2D aggregates were domains of the ordered monolayer of the fluorescent dye molecule 3,4,9,10-perylenetetracarboxylic acid dianhydride on a KCl(100) surface. Fluorescence and fluorescence excitation (FLE) spectra were measured as a function of temperature. The system shows a pronounced superradiant emission which yields additional information on the number of coherently coupled molecules participating in the emission. From calculations of the spectra within the tight binding model we find that the finite size of the 2D ordered domains of about  $N = 7 \times 7$  molecules, in combination with a Poissonian domain-size distribution, explains the line profile. Line broadening mechanisms due to site disorder or thermal effects – although not excludable straightaway – are not needed to explain the observed FLE line profile. This yields insight into the important, but so far not well understood, relation between the line profile and the size of ordered molecular aggregates. © 2013 AIP Publishing LLC. [<http://dx.doi.org/10.1063/1.4813521>]

## I. INTRODUCTION

The understanding of the line shapes in fluorescence (FL) or absorption spectra of molecular aggregates is of fundamental interest because it bears information on the coupling of the molecular entities and the resulting delocalization of optical excitations.<sup>1,2</sup> These aspects deserve attention for the design of organic devices interacting with light, e.g., organic light emitting devices (OLEDs) or organic solar cells (OSCs).<sup>3</sup> For instance, the exciton diffusion length in molecular aggregates which is relevant for OSCs is directly related to the strength and type of the intermolecular coupling of the optical excitations in the aggregates.<sup>4</sup>

An important class of aggregates is given by the so-called *J-aggregates*, which are characterized by a redshift of the absorption spectrum with respect to the monomer spectrum and a superradiant emission.<sup>5</sup> In contrast to the individual monomers, the J-aggregate absorption and emission spectra show only weak vibronic features and are dominated by a strong single peak corresponding to the pure electronic, i.e., the 0-0 transition. This peak is often named the “J-band”. Typically the J-band is much narrower than the respective line in the spectrum of the individual monomers,<sup>6</sup> which is usually broadened, e.g., by coupling to low energy vibrations or different local environments. The appearance of the J-band and the corresponding superradiant emission are due to transition dipole-dipole interactions between the monomers which lead to states where the electronic excitation is coherently delocalized over many monomers. For ideal periodic and infi-

nite aggregates, i.e., crystals, these states are Frenkel excitons and exhibit a specific dispersive band structure in  $k$ -space.<sup>7</sup> The optical transitions are only allowed as vertical transitions ( $\Delta\mathbf{k} = 0$ ) and, for ideal crystals, yield sharp lines. For crystals with a structure related to that of J-aggregates the respective transition is located at the  $\Gamma$  point and at the bottom of the exciton band.<sup>5</sup>

However, for aggregates of limited size the exciton band structure model is no longer strictly valid and the spectra have to be calculated for aggregates of a limited number ( $N$ ) of coupled molecules. As a consequence several transitions that are spread over a small energy range gain oscillator strength, in contrast to crystals where only singular transitions are allowed due to selection rules. As we will demonstrate in this work, the splitting of the exciton transition into several close-spaced transitions occurs due to the finite size of the aggregates. However, the individual close-spaced transitions can (in our case) experimentally *not* be resolved. They are smeared out in the experimental situation due to the distribution of the size of aggregates on the sample. As an effect, the single and sharp line profile of the infinite aggregate is broadened and becomes considerably asymmetric due to this finite size effect.

In addition to the line broadening, the sample investigated here shows a second effect, namely superradiance (SR). With SR we refer to the enhancement of the radiative decay in the aggregate compared to that on a single molecule caused by coherent emission of several molecules. The corresponding *enhancement factor* will be denoted by  $N_c$ . SR has been studied so far mainly for molecular organic crystals<sup>8</sup> or aggregates of self-organized dye molecules in liquids.<sup>9</sup> Recently, the coherent length of excitons in J-aggregates has been investigated

<sup>a)</sup> Author to whom correspondence should be addressed. Electronic mail: sokolowski@pc.uni-bonn.de. Tel.: +49 (0)228-73 2507. Fax: +49 (0)228-73 25511.

by two-dimensional Fourier transform spectroscopy.<sup>10</sup> The present example is to our knowledge the first where SR has been studied for a two dimensional (2D) aggregate realized in the form of a monolayer of molecules adsorbed on a well-defined surface. As it turns out, the SR yields an independent possibility to estimate the number of coherently interacting molecules. For a perfectly delocalized Frenkel exciton ground state the number of interacting molecules is just  $N = N_c$ . In general, however,  $N_c$  is smaller than the number  $N$  of interacting molecules. The number  $N_c$  hence sets a lower limit to the possible size of the aggregate that has to be considered when interpreting the broadening of the lines by a finite size effect.

In detail, we have measured the temperature dependent line profiles of the optical transition of ordered domains in the monolayer of the fluorescent model molecule 3,4,9,10-perylenetetracarboxylic acid dianhydride (PTCDA) on a surface. These domains are 2D J-aggregates concerning their optical properties, and we hence use the terms aggregates and domains synonymously here. From calculations in the tight binding model performed on aggregates of finite size we were able to explain the experimental line profiles.

## II. EXPERIMENTAL

The aggregates were produced by deposition of PTCDA on a thin epitaxial KCl(100) film. The latter was grown before on an Ag(100) single crystal surface. The experimental details are described in Ref. 11. The structural characterization of the aggregates was performed by low energy electron diffraction (LEED). This was done after the optical experiments in order to avoid effects in the optical spectra by possible electron beam damages. Notably, all experiments were performed *in situ* under ultra-high vacuum.<sup>12</sup> The lowest achievable sample temperature was 20 K. For recording the FL and fluorescence excitation (FLE) spectra an Ar<sup>+</sup>, respectively a cw dye laser, was used. Typical excitation powers were in the range of 10–100 mW. The FL light was measured with a spectrometer equipped with a liquid nitrogen cooled CCD camera. For the FLE spectra the FL intensity at a specified detection wavelength ( $\lambda_{\text{det}}$ ) was plotted versus the excitation wavelength ( $\lambda_{\text{exc}}$ ) of the laser. These FLE spectra correspond to the respective absorption spectra.<sup>12</sup> The instrumental broadening in the FLE spectra is determined by the spectral width of the dye laser ( $\sim 3 \text{ cm}^{-1}$ ) and is small. The experimental resolution of the FL spectra is determined by the spectrometer and amounts to  $\sim 30 \text{ cm}^{-1}$  (grating of 300 grooves/mm). Further experimental details can be found in Refs. 11, 13, and 14.

To create the aggregates, a monolayer of PTCDA was deposited at a substrate temperature of 260 K.<sup>11</sup> At this temperature, the surface mobility of PTCDA is high and self-organization leads to growth of domains with a commensurate, long-range ordered structure with one molecule per unit cell, as illustrated in Fig. 1. This structure is often referred to as the *brickwall (BW) structure* of PTCDA which differs from the herring-bone structure of PTCDA present in bulk lattice planes.<sup>15</sup> The commensurability is induced by electrostatic interactions between the positively charged potassium cations of the KCl(100) surface and negatively charged oxygen atoms of PTCDA.<sup>16</sup> The transition dipole  $\mu$  of the optical

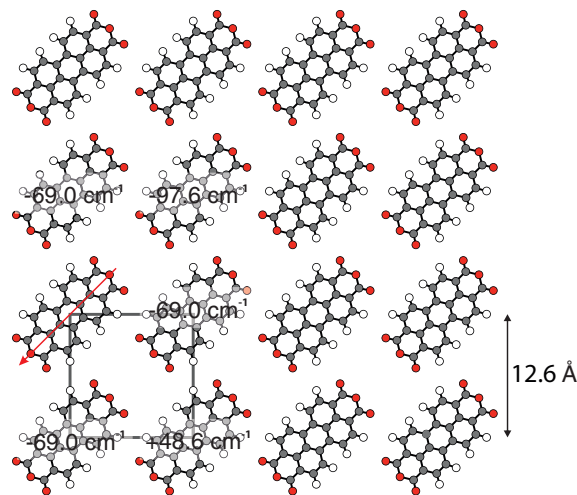


FIG. 1. Schematic presentation of a domain of finite size ( $4 \times 4$ ) of the brickwall (**BW**) phase of PTCDA with indicated unit cell. The  $S_0/S_1$  transition dipole is indicated on one molecule. In addition interaction energies of this molecule with next neighbor and next-next neighbor molecules are given.

$S_0$ - $S_1$  transition is oriented along the long molecular axis.<sup>17</sup> A remarkable and important aspect of the **BW** structure is the parallel orientation of the transition dipoles. The consequence of this arrangement will be discussed below.

Due to the substrate symmetry, two  $90^\circ$  rotational domains, and due to the size of the unit cell 8 different translational domains exist. As a result of kinetic limitations during the growth process and surface defects, e.g., steps, a monolayer consists of many ordered domains of finite size, separated by phase boundaries. From LEED we derived that the domains exhibit an average diameter  $L$  of about  $100 \text{ \AA}$ ,<sup>11</sup> which corresponds roughly to a domain with  $7 \times 7$  PTCDA molecules.

In addition to the condensed **BW** phase, as a reference, a diluted (**d**) phase consisting of isolated PTCDA molecules was prepared by depositing a very small coverage of molecules ( $< 1\%$  of a monolayer) onto the KCl substrate at a temperature of 20 K. At this temperature the surface diffusion is so small that condensation into ordered domains is suppressed and the molecules remain statistically distributed as isolated molecules on the surface.

## III. RESULTS AND DISCUSSION

### A. General overview on the spectral changes due to aggregation

We start with an overview on the optical spectra. Fig. 2 displays the fluorescence FL and FLE spectra of the **d** (bottom) and the **BW** phase (top). The spectra show a dominating pure electronic transition (0-0 transition), which is found at  $20\,000 \pm 20 \text{ cm}^{-1}$  and  $19\,600 \pm 20 \text{ cm}^{-1}$ , for the **d** and **BW** phase, respectively. The spectra of both phases show well resolved molecular vibronic modes, which are mainly related to in-plane modes of the flat lying molecule.<sup>13</sup>

For the spectra of the **d** phase, consisting of isolated molecules, most of the vibronic modes are in excellent

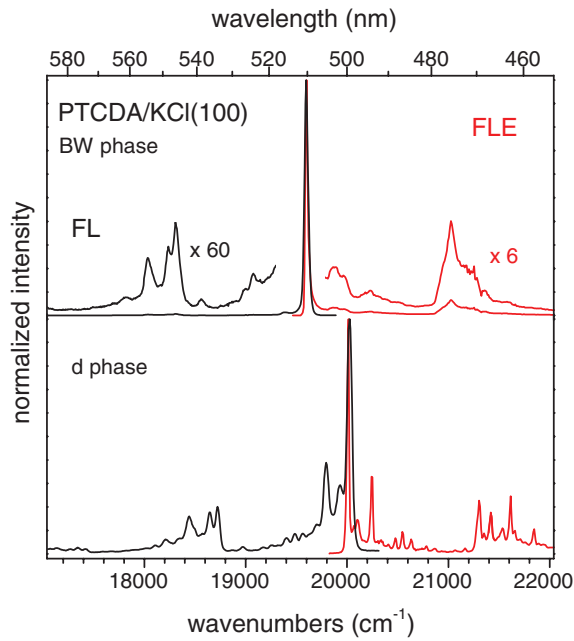


FIG. 2. Fluorescence (FL) and fluorescence excitation (FLE) spectra of PTCDA in the **BW** (top) and the diluted (**d**) phase (bottom), both measured at a cryostat temperature of 20 K. The excitation wavelengths were 471 nm and 465 nm, respectively, whereas the detection wavelength ( $\lambda_{\text{det}}$ ) for the FLE spectra was 555 nm and 534 nm, respectively.

agreement with those of isolated, non-interacting PTCDA molecules (monomers) studied in He nano-droplets.<sup>18</sup> This reveals that the distortion of the potential energy surface due to the adsorption on the surface is small. Only few modes are slightly ( $\leq 15 \text{ cm}^{-1}$ ) affected by the molecule/surface interaction, and some low energy vibronic modes couple additionally to the transition due to the surface bonding, as discussed in detail in Ref. 13. Notably, the absolute positions of the 0-0 transition of the **d** phase is redshifted by  $980 \text{ cm}^{-1}$  with respect to that for PTCDA in Helium nano-droplets (at  $20980 \text{ cm}^{-1}$ ). Hence, under the assumption that the polarizability of He can be neglected, we can quantify the redshift of the optical transition due to the polarizability of the underlying KCl substrate by  $980 \text{ cm}^{-1}$ .

The comparison of the spectra of the two phases shows three differences which are all related to the intermolecular coupling of the molecules, present in the **BW** phase, but negligible in the **d** phase due to the larger intermolecular distances. First of all, a shift of the 0-0 transition energy  $\Delta E^{\text{BW/d}} = -400 \text{ cm}^{-1}$  to lower energies is found for the condensed **BW** phase with respect to the **d** phase. Second, at 20 K, the relative intensities of the vibrational lines of the spectra of the **BW** phase are drastically reduced with respect to those of the **d** phase, in FL by about a factor of 30 (respectively 20, if the integrated peak intensities are considered) and in FLE by a factor of 3. This effect demonstrates the above noted SR and will be dealt with in detail below. The difference between the mode suppression in the FL and FLE spectra will be subject of a forthcoming publication. And third, the good mirror symmetry of the energetic positions of the vibrational modes in the FL and FLE spectra with respect to the 0-0 transition, which is present for the **d** phase, is lost for

the **BW** phase, as can be seen, e.g., for the vibronic modes between  $21000$  and  $21400 \text{ cm}^{-1}$ . This latter observation was also made by *Dienel et al.* before.<sup>16</sup> In the following we will only consider the first and second effect. The third effect will be dealt with in a separate publication.<sup>19</sup>

## B. Calculation of transition energies

The electronically excited states in aggregates can be described within first order perturbation theory in the interaction between the monomers.<sup>7</sup> Since the direct overlap of the molecular wavefunctions of different monomers is small, it is possible to ignore electron exchange and the respective electronic exciton Hamiltonian in the one-exciton subspace is

$$H = \sum_n (E_0 + D_{\text{mol}}) |n\rangle \langle n| + \sum_{m,n \neq m} J_{mn} |m\rangle \langle n|. \quad (1)$$

Here  $|n\rangle = |\varphi_n^e\rangle \prod_{m \neq n} |\varphi_m^g\rangle$  denotes the product wavefunction of an aggregate with  $N$  molecules, where the molecule  $n$  is electronically excited ( $|\varphi_n^e\rangle$ ) and all other molecules ( $m \neq n$ ) are in the ground state ( $|\varphi_m^g\rangle$ ).<sup>20,21</sup>  $E_0$  is the excitation energy of the isolated molecule.  $D_{\text{mol}}$  denotes an energy shift due to non-resonant interactions between the molecules. For an aggregate of finite size this term is in general site dependent, but we will not treat this effect explicitly, since we believe that its variation is quite small within the aggregate. The non-resonant interaction of the molecules with the substrate will also not be treated explicitly.

The second term in Eq. (1) contains the intermolecular coupling that is responsible for the transfer of excitation energy between the molecules. To a good approximation the transition matrix elements  $J_{mn}$  are given by the interaction energies of point-like transition dipoles<sup>22</sup>

$$J_{mn} = \frac{1}{4\pi\epsilon_0} \left( \frac{\boldsymbol{\mu}_m \boldsymbol{\mu}_n}{r^3} - 3 \frac{(\boldsymbol{\mu}_m \mathbf{r})(\boldsymbol{\mu}_n \mathbf{r})}{r^5} \right), \quad (2)$$

whereby  $\mathbf{r}$  is the vector pointing from the molecule  $n$  to molecule  $m$  with respective transition dipole moments  $\boldsymbol{\mu}_n$  and  $\boldsymbol{\mu}_m$ . We used  $|\boldsymbol{\mu}_n| = \mu^0 = 7.4 \text{ D}$ .<sup>23</sup> The respective interaction energies ( $J_{mn}$ ) resulting for next neighbored and next-next neighbored molecules are indicated in Fig. 1.

In the present work we will not explicitly take the coupling of the electronic excitation to vibrational modes of the molecules into account. For large aggregates and many vibrational modes this is a formidable task (see, e.g., Refs. 22, 24). Here we will focus on the purely electronic Hamiltonian given by Eq. (1), taking the influence of vibrations into account only implicitly. Since the matrix elements  $J_{mn}$  are small compared to the frequencies of the PTCDA vibrations, the 0-0 transition will only weakly couple to vibronic transitions. Therefore we introduce the rescaled interaction  $\tilde{J}_{mn} = \chi^2 J_{mn}$  for the interaction between two monomers in Eq. (1), where  $\chi^2 = \chi^2_{\nu\nu'}$  denotes the Franck-Condon-factor of the 0-0 transition,  $\nu = \nu' = 0$ . We determine  $\chi^2$  from the spectrum of the **d**-phase and obtain  $\chi^2_{00} = 0.21$ .<sup>13</sup> We note that this latter value is smaller to the one we used in Ref. 25 ( $\chi^2_{00} = 0.42$ ), since the present value was taken from a recent more accurate evaluation of the vibronic fine structure.<sup>13</sup>

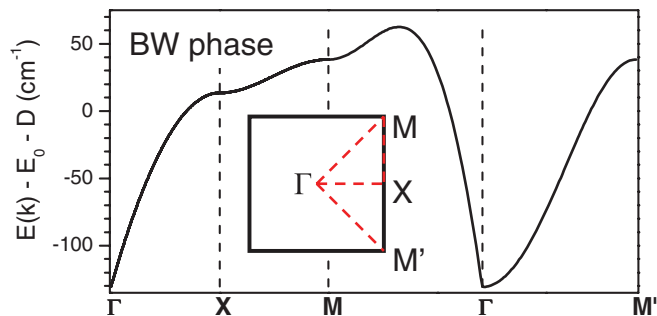


FIG. 3. Exciton band structure of the **BW** phase, calculated for a very large ( $400 \times 400$  molecules) domain and representation of the Brillouin zone.

The eigenstates of Eq. (1) can be written as  $|l\rangle = \sum_n c_{l,n} |n\rangle$ , with  $l = 1 \dots N$ . In the limit of a large aggregate with a periodic structure, the eigenstates  $|l\rangle$  are Bloch states that yield a bandstructure  $E(\mathbf{k})$ .<sup>21</sup> We have calculated  $E(\mathbf{k})$  for an aggregate of the type shown in Fig. 1 using  $\tilde{N} = 400$  monomers in both directions. By varying  $\tilde{N}$  we checked that finite size effects are negligible in this range of  $\tilde{N}$  and hence a good approximation of the infinite aggregate is obtained. The so calculated exciton band structure is shown in Fig. 3. It exhibits a minimum at the  $\Gamma$  point as it is expected for a J-aggregate.<sup>5</sup> At the  $\Gamma$  point, the strongest dispersion ( $\partial E/\partial \mathbf{k}$ ) is found along the  $\Gamma M$  direction, i.e., the direction along the long molecular axis. This is in accordance with the attractive head-to-tail interaction between the transition dipoles in this direction (cf. Fig. 1). Notably, the attractive coupling is also supported by the shift by half a molecular length between the rows which causes an attractive coupling between next neighboring molecular rows in addition to the attractive coupling within the rows.<sup>5</sup>

Due to the negligible momentum of the photon and the conservation of  $\mathbf{k}$ , optical transitions occur only at the  $\Gamma$  point of the exciton band structure. The calculated energy gain at the  $\Gamma$  point due to the exciton band formation is  $\Delta E = E(\mathbf{k} = 0) - (D_{\text{mol}} + E_0) = -130 \text{ cm}^{-1}$ . The experimentally observed energy shift of the 0-0 transition between the **BW** and **d** phase is  $\Delta E^{\text{BW/d}} = -400 \text{ cm}^{-1}$ . There are two contributions to this shift. One is given by the noted energy  $\Delta E = -130 \text{ cm}^{-1}$  related to the exciton band formation. The other ( $\Delta E^{\text{BW/d}} - \Delta E = -270 \text{ cm}^{-1}$ ) is attributed to the difference of the term  $D_{\text{mol}}$  of the two phases, i.e., to the non-resonant interactions between the PTCDA molecules (see Eq. (1)). For the **d** phase, the term  $D_{\text{mol}}^{\text{d}}$  is only very small due to the small density of the molecules and the resulting large intermolecular distances. It can be neglected with respect to  $D_{\text{mol}}^{\text{BW}}$  and hence  $-270 \text{ cm}^{-1} = D_{\text{mol}}^{\text{BW}} - D_{\text{mol}}^{\text{d}} \approx D_{\text{mol}}^{\text{BW}}$ . However, in combination with site disorder  $D_{\text{mol}}^{\text{d}}$  can lead to small energy shifts which contribute to the line broadening (see below). We note that we found a comparable situation also for a condensed PTCDA layer on NaCl(100).<sup>25</sup>

### C. Line shape of the 0-0 transition

We now turn to a more detailed discussion of the line shape of the 0-0 transition at 20 K. For this purpose the line

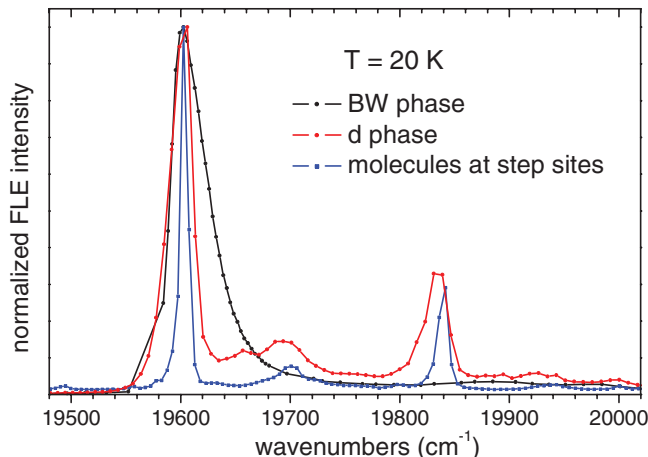


FIG. 4. Comparison of the 0-0 line shape in the fluorescence excitation (FLE) spectra of the **BW** and the **d** phase at 20 K ( $\lambda_{\text{det}} = 625 \text{ nm}$  and  $534 \text{ nm}$ , respectively). The spectrum of the **d** phase was shifted by  $-405 \text{ cm}^{-1}$  for alignment of the peak maxima. The absence of the vibronic modes in the spectrum of the **BW** phase, that are seen for the **d** phase, e.g., at  $19660$ , and  $19700 \text{ cm}^{-1}$ , and  $19840 \text{ cm}^{-1}$  is due to the superradiance of the **BW** phase. In addition, a spectrum of a very diluted phase, where the molecules are solely adsorbed at steps sites, is displayed for comparison to illustrate the site broadening of the spectrum of the **d** phase. The peak position of this spectrum was shifted by about  $-535 \text{ cm}^{-1}$ . For further details see text.

profiles of FLE spectra measured for the condensed **BW** and for isolated molecules in the **d** phase are compared on an extended scale in Fig. 4.

The line profile of the **d** phase is about *symmetric* and has a full width at half maximum (FWHM) of  $27 \text{ cm}^{-1}$ . Contributions to the line width related to the finite life time<sup>26</sup> of the excited state or the width of the laser profile ( $\sim 3 \text{ cm}^{-1}$ ) can be neglected. Relevant contributions are *thermal* line broadening (dephasing) and *inhomogeneous* line broadening due to site disorder. The site disorder is the dominating effect here and results from the statistical distribution of the molecules on the surface. It comprises variations of the intermolecular distances and the distances of the molecules with respect to steps and defects of the KCl surface. Both aspects lead to small variations in the interactions of the molecules with their environment (resonant and non-resonant), which cause a broadening of the line. Experimental evidence for the importance of the site disorder is given by the observation that the FLE line profile narrows considerably ( $\sim 8 \text{ cm}^{-1}$ ), when the molecules are selectively adsorbed at KCl step edges.<sup>14</sup> A corresponding spectrum is shown in Fig. 4. The details of this spectrum are reported in Ref. 14. We further note that, since the molecules are spatially isolated, soft molecular lattice phonons are not present for the **d** phase.

The line profile of the **BW** phase is *asymmetric* and shows an extended wing on the high energy side, which is not present for the line profile of the **d** phase (see Fig. 4). Most notably the width of the peak in the **BW** phase is much broader than that of the **d** phase. In detail, the asymmetric line profile **BW** phase exhibits a half width at half maximum of about  $10 \text{ cm}^{-1}$  on the low, and  $30 \text{ cm}^{-1}$  on the high energy side (yielding a total FWHM of  $40 \text{ cm}^{-1}$ ). While an

asymmetric line-shape is common for the J-band,<sup>5,6,27</sup> the amount of the broadening with respect to the monomer line width is remarkable. In fact, from *exchange narrowing* arguments<sup>28</sup> one would expect that the J-band width is *narrowed* compared to the line of the monomer by a factor of roughly  $1/\sqrt{N_{\text{coh}}}$ , where  $N_{\text{coh}}$  is the number of molecules over which the excitation is coherently delocalized. Clearly this is not the case here. Hence there is the question on the physical origin of this difference in the line profiles of the two phases.

#### D. Calculations for domains of finite size

We propose a finite size effect related to the limited spatial extension of the domains. The domains are limited by domain boundaries which terminate the periodic arrangement of the molecules. The domain boundaries may either result from incoherent nucleation of different translational or rotational domains on the surface during the growth or from steps of the KCl surface that limit the lateral extension of the PTCDA domains. Experimentally the limited domain size is observed by the broadening of the LEED profiles (see Sec. II).

In order to demonstrate the finite size broadening in the optical spectra we have calculated the transition probabilities for domains of finite size using the Hamiltonian of Eq. (1). While the orientation of the molecules within one domain is known from LEED measurements, the details of domain boundaries, in particular their preferential orientations, are not exactly known. For our calculations we used rectangular domains of the type illustrated in Fig. 1. The illustrated domain boundaries are plausible from energetic aspects, because other domain boundaries, e.g., those rotated by  $45^\circ$  with respect to the illustrated, would be terminated either by only negatively charged anhydride groups or by only positively charged hydrogen terminated sides of perylene cores. This would yield polar, and hence from electrostatic arguments, energetically unfavorable boundaries. In addition, the anticipated orientation of the domain boundaries is identical to that of the energetically preferred non-polar steps on the KCl(100) surface, which can act as nucleation and limitation lines for the PTCDA domains, as observed on the NaCl(100) surface.<sup>29</sup> This orientation of the PTCDA domain boundaries on KCl(100) was also seen by *Dienel et al.*<sup>16</sup> In our calculations we considered isolated domains, where no coupling between molecules across domain boundaries occurs and also a possible local variation of the term  $D_{\text{mol}}$  was neglected. In reality, the patchwork of the different PTCDA domains covers the surface completely, and hence some coupling between neighboring domains is likely. Hence our calculations have to be understood as model calculations comprising only basic aspects of the real system. Concerning the domain size distribution we proceeded in two steps: In the first step we considered domains of only one single size. In the second step, a distribution of domains with different sizes was used.

##### 1. Single size aggregates

The spectra calculated for three exemplary quadratic domains of  $N = \tilde{N} \times \tilde{N}$  molecules, with  $\tilde{N} = 4, 7,$  and  $15$  are

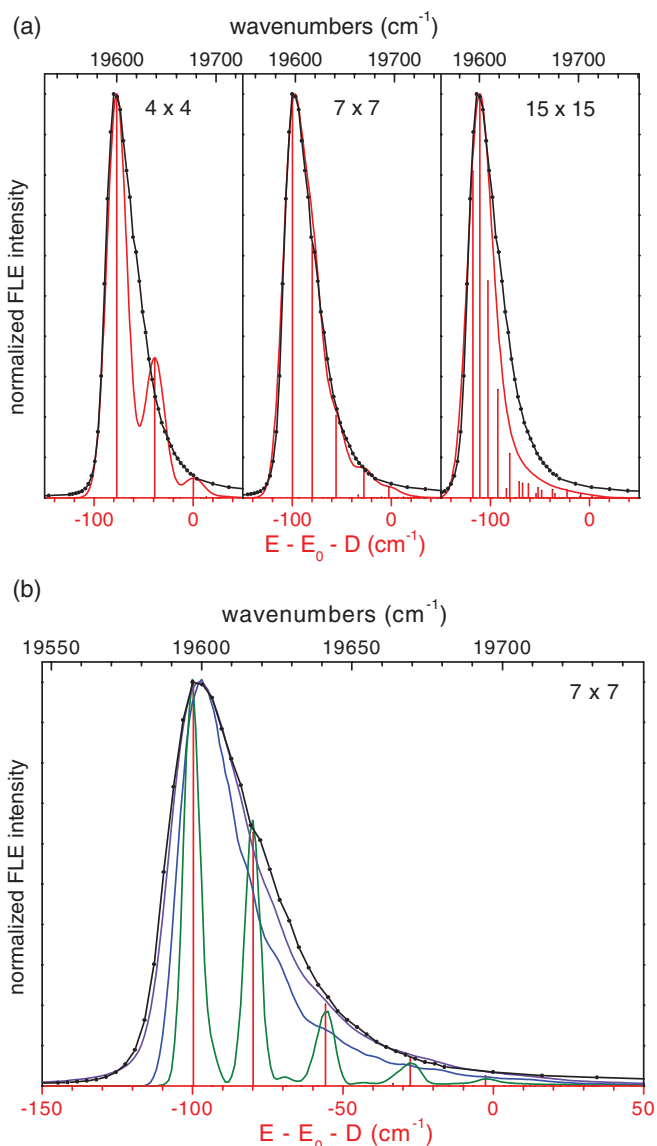


FIG. 5. (a) Comparison of the experimental FLE spectrum (black) of the **BW** phase at 20 K and  $\lambda_{\text{det}} = 658$  nm (black) and calculated spectra for three domains of different sizes ( $\tilde{N} \times \tilde{N}$ ) (red) with  $\tilde{N} = 4, 7,$  and  $15$ . The experimental and calculated spectra were aligned at the positions of the peak maxima. For further details see text. (b) Comparison of the experimental FLE spectrum (black) of the **BW** phase as above with calculated spectra. The red stick spectrum is the spectrum for a single domain of  $7 \times 7$  molecules. The green spectrum includes additional site disorder. The blue spectrum is the spectrum for a Poissonian distribution of domain sizes with the mean of 7 in the  $x$  and  $y$  directions. The purple spectrum is obtained from the blue by convolution with a Lorentzian with a FWHM of  $5 \text{ cm}^{-1}$ .

shown in Fig. 5(a). They consist of several transitions of different intensity which belong to different eigenstates  $|l\rangle$ . The respective intensities  $I_l$  are proportional to  $\mu_l^2$ , whereby  $\mu_l = \sum_n c_{l,n} \mu_n^0$ . Hence, in contrast to the infinite aggregates, for the finite size aggregates we find several strong transitions at the bottom of the exciton band. They are indicated by the stick spectra. Remarkably, the intensity variation of the stick spectra describes the asymmetric line shape very well, and in particular the wing on the high energy side, of the experimentally observed line profile. Hereby the individual transitions are the closer in energy the larger  $N$

becomes and shift to lower energies with increasing  $N$ , since more and more molecules contribute to the excitonic coupling. Note that for  $\tilde{N} = 15$ , we read from Fig. 5(a)  $\Delta E = E(\mathbf{k} = 0) - (D_{\text{mol}} + E_0) = -120 \text{ cm}^{-1}$  for the line at lowest energy. This amounts to about 92% of the value of  $-130 \text{ cm}^{-1}$ , which was calculated above for the domains of “infinite” size ( $\tilde{N} = 400$ ).

For large  $N$  the profile converges to a single line, which is plausible, since in the limit of large  $N$  the case of an exciton band structure with a single transition located at the  $\Gamma$  point must be obtained. To facilitate comparison to the experimental spectrum the sticks have been convoluted by a Gaussian with a FWHM of  $24 \text{ cm}^{-1}$ , which is close to the FWHM of the 0-0 line of the **d** phase ( $27 \text{ cm}^{-1}$ ). The convolution with the Gaussian smears out the stick spectrum and makes it similar to the experimentally observed spectrum. This smearing comprises several physical effects which will be explained further below. At present, we concentrate on the effect of the domain size only. An excellent simulation of the experimental line profile is achieved for  $\tilde{N} = 7$  (see Fig. 5(a)). The domain of  $N = 7 \times 7$  molecules has a size of  $88 \text{ \AA} \times 88 \text{ \AA}$ . This size agrees very well to the average domain diameter that is deduced from the width of the LEED spots, i.e.,  $100 \text{ \AA}$ .

## 2. Influence of static disorder

Obviously, the effects that smear out the stick spectra deserve further attention. The first effect we consider is site disorder, ignoring finite temperature and coupling to vibrations for the moment. As we will demonstrate, site disorder has only a small effect on the line width in the case of aggregates, in contrast to the case of isolated molecules. We modeled the site disorder by introducing diagonal disorder into the Hamiltonian (Eq. (1)).<sup>27</sup> Numerically, we did this by calculating the respective stick spectra for a large set of different Hamiltonians, which were obtained by statistically adding small energies to the diagonal elements according to a Gaussian distribution with a FWHM of  $27 \text{ cm}^{-1}$ . This value was motivated from the observed FWHM of the 0-0 transition of the **d** phase, assuming that the site disorder of the **BW** phase is of the same size as that of the **d** phase, which appears to be reasonable. We note that in this model we also assume that the site energies of molecules in the **BW** phase are uncorrelated with the local positions of the molecules within the domain, which likely is not the case in reality. The modeling is hence indeed very crude, but it demonstrates the important effect.

The resulting line profile is shown as the green line in Fig. 5(b). We obtain nearly the same spectrum as without site disorder. The peaks are only slightly broadened and have a FWHM of  $6\text{--}8 \text{ cm}^{-1}$ . Remarkably, this broadening is much smaller than the width of the Gaussian describing the site disorder which was included in the calculation ( $\Delta_{\text{disorder}} = 27 \text{ cm}^{-1}$ ). This is due to the well known phenomenon of *exchange narrowing* of the line width in the aggregate due to the delocalisation of the excitation on  $N_{\text{coh}}$  molecules.<sup>1,28</sup> In the present case of a  $7 \times 7$  domain, the spacing between unperturbed eigenstates is so large that the disorder does not mix different unperturbed eigenstates (which we have confirmed

numerically). Given this we can estimate that the line width is reduced by roughly a factor  $\kappa = 1/\sqrt{N_{\text{coh}}}$  with respect to that of the uncoupled monomers. In the present case we have  $\kappa = 0.22 = 6 \text{ cm}^{-1}/27 \text{ cm}^{-1}$  from the ratio of the respective FWHMs (of the two FLE peaks at lowest energies, cf. Fig. 5(b)) and  $\kappa = 0.30 = 8 \text{ cm}^{-1}/27 \text{ cm}^{-1}$  for the third peak. This implies  $N_{\text{coh}} = \kappa^{-2}$  to be of the order of 20 and 11, respectively. The small difference between the  $N_{\text{coh}}$  values of the different peaks can be understood from the difference in the spatial locations of the respective wavefunctions.

## 3. Aggregates with different sizes

As a consequence, site disorder cannot explain the experimentally observed line broadening for the aggregates, nor is it sufficient to explain the smearing out of the spectra that results from the finite size of the aggregates. There must be another effect, which leads to the smearing out of the stick spectra. We identified the broadening as an effect from the presence of aggregates with a certain distribution in their sizes, i.e., of  $N = \tilde{N}_x \times \tilde{N}_y$ . Since the aggregates are domains of ordered molecules, we will refer to this distribution also as the domain size distribution. To model line shapes of a sample with a distribution of domains of different sizes we averaged spectra that were calculated for a large number of domains, where the probabilities of  $\tilde{N}_x$  and  $\tilde{N}_y$  follow Poissonian distributions ( $p(\tilde{N}_{x,y}) = (\lambda^{\tilde{N}_{x,y}}/\tilde{N}_{x,y}!) \exp(-\lambda)$ ) with a mean of  $\lambda = 7$ . Notably, this 2D Poissonian domain size distribution also includes domains of rectangular shape, although it is symmetric in  $x$  and  $y$ . It should be understood as a model distribution that demonstrates the effect. Likely, the true distribution will be somewhat different and depend on the exact preparation conditions. However, recent model calculations of the LEED profiles of the PTCDA domains revealed that this type of a Poissonian domain size distribution fits the experimental LEED profiles and is hence compatible with these.

The result is shown as the blue curve in Fig. 5(b). Obviously the stick spectrum is smeared out very effectively and a good agreement with the experimental spectrum is obtained. A nearly perfect agreement is obtained when the spectrum is finally convoluted by a Lorentzian of  $\text{FWHM} = 5 \text{ cm}^{-1}$  (purple curve in Fig. 5(b)). This Lorentzian function was found by trial and error and effectively summarized so far not encountered smaller broadening effects, as, e.g., the width of the laser line and thermal line broadening (see also below). It yields only a small modification of the line profile calculated for the sample with different domain sizes. In conclusion we find that the finite size of the domains together with the distribution of the domain sizes leads to the broadening and the asymmetric shape of the line profile.

## E. Superradiance

As mentioned above, the decrease of the vibronic modes in the FL and FLE spectra with respect to the pure electronic transition of the **BW** phase is due to the forming of a coherent and delocalized exciton ground state. In emission this leads to superradiance (SR). In this context, the finite size of the

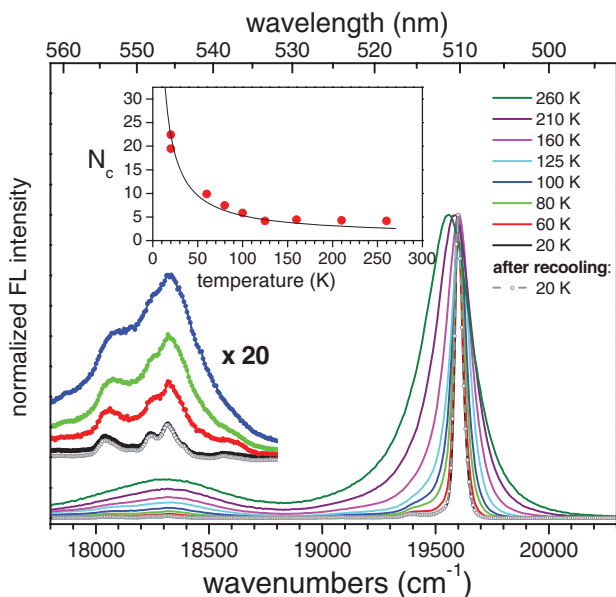


FIG. 6. Fluorescence spectra of the **BW** phase as a function of temperature demonstrating the superradiance. The excitation wavelength was 476 nm. The inset shows the number of coherently emitting molecules  $N_c$  determined from the enhancement of the 0-0 transition with decreasing temperature. For further details see text.

aggregates has an important consequence: It limits the maximal achievable enhancement of the SR, because the enhancement factor  $N_c$  can principally not exceed the number of monomers  $N$  of the aggregates, even for vanishing temperature. Hence, the factor  $N_c$  deduced from the SR should never exceed the domain-size that we have estimated above, i.e.,  $N_c \leq N$  should hold. Thus the following discussion of SR is also a consistency check of the domain-size obtained above from the absorption line shape.

Since in our experimental setup we cannot measure the time-dependence of the fluorescence decay (which would directly give the enhancement factor  $N_c$ ) we use the procedure of Ref. 30 to extract this factor from computing the enhancement of the integrated intensity of the 0-0 transition with respect to that of the vibronic transitions. The enhancement of the 0-0 line with respect to the vibronic modes in the FL spectrum is proportional to the enhancement factor  $N_c$  which is roughly the number of molecules that are coherently coupled.<sup>31</sup> Besides a finite size of the aggregate,  $N_c$  can also be limited by energetic disorder or by thermal destruction of the coherence. Due to the second effect,  $N_c$  is reduced at elevated temperatures, leading to a breakdown of the SR. This is observed for the present system in Fig. 6.

Extending the procedure proposed for one vibrational mode in Ref. 30 we determined  $N_c$  by computing the enhancement of the integrated intensity of the 0-0 transition with respect to that of the first vibronic sideband (18036–18318  $\text{cm}^{-1}$ ), which comprises several vibronic transitions. In order to eliminate the contribution of the Franck Condon factor, the values for the **BW** phase were normalized by those of the **d** phase which is not superradiant, since in this phase the molecules are not close enough to each other to couple effectively. The resulting values of  $N_c$  as a function of temperature are shown in the inset of Fig. 6. They show the expected

strong temperature dependence and a good fit by  $N_c = 1 + E_B/k_B T$  can be obtained with using a value  $E_B = 400 \text{ cm}^{-1}$  for the energy parameter  $E_B$  of the coherent state as discussed in Ref. 30. At 20 K we estimate a value of  $N_c$  of  $\sim 20$  from Fig. 6. Notably, this number is consistent with the estimated number of  $N = 49$  molecules in a typical  $7 \times 7$  domain, since  $N_c < N$  holds, as it should be. Note that for a  $7 \times 7$  domain at zero temperature the radiative enhancement obtained determined theoretically from the eigenfunction of the lowest exciton state is  $N_c^{0\text{K}} \sim 25$ . Because of finite size effects this value is considerably smaller than the number  $N = 49$  of coherently coupled monomers. On the contrary, it fits well to the number  $N_c \sim 20$  obtained from Fig. 6. We note that  $N_c$  is also roughly consistent with the value  $N_{\text{coh}} = 11$  estimated from the exchange line narrowing, since we find  $N_c \sim 2 \times N_{\text{coh}}$ .

## F. Aspects concerning thermal line broadening

Finally, we make some remarks about the thermal line broadening. Generally, thermal line broadening is caused by dephasing of the excitation due to scattering of the excitons with phonons.<sup>32</sup> For the present sample the phonons may be either substrate phonons or phonons of the condensed molecular layer itself. The details of the phonon spectrum will vary for the specific samples and the different related phonon densities. Differences can be hence expected, for instance, for the isolated molecules (d phase) and the condensed BW phase which we consider here. Obviously, temperature induced broadening could constitute an alternative mechanism to the postulated finite size effect to interpret the line broadening. The purpose of the following discussion is to describe the thermal line broadening and to consider the arguments which yield indications against a dominant thermal line broadening at 20 K. However, as it will turn out, due to the complexity of the dephasing, some caution remains and we will not be able to make a definite decision at the end.

A first aspect to be noted concerns the asymmetry of the line profile. In contrast to the so far described finite size effect which explains the *asymmetric* line broadening at low temperatures, we find that the thermal line broadening at higher temperatures by interactions with phonons, which are not further specified so far, leads to a *symmetric* line broadening. This can be seen in Fig. 7, where three exemplary FLE line profiles at different elevated temperatures (100 K, 160 K, and 260 K) are shown. This qualitative difference in the line shape is a first indication that thermal line broadening is unlikely the dominant broadening mechanism at 20 K.

In Ref. 27 it has been suggested that the thermal broadening can be modeled by introducing diagonal disorder into the Hamiltonian (Eq. (1)). Numerically, we did this by calculating the respective stick spectra for a large set of different Hamiltonians, which were obtained by adding small energies to the diagonal elements according to a Gaussian distribution with a standard deviation of  $\Delta\epsilon$ . We note that for simplicity, we considered only aggregates of identical size  $N = 7 \times 7$  here. The broadening related to the presence of domains of different sizes was hence neglected in this analysis; in addition, the small broadening related to site disorder (included

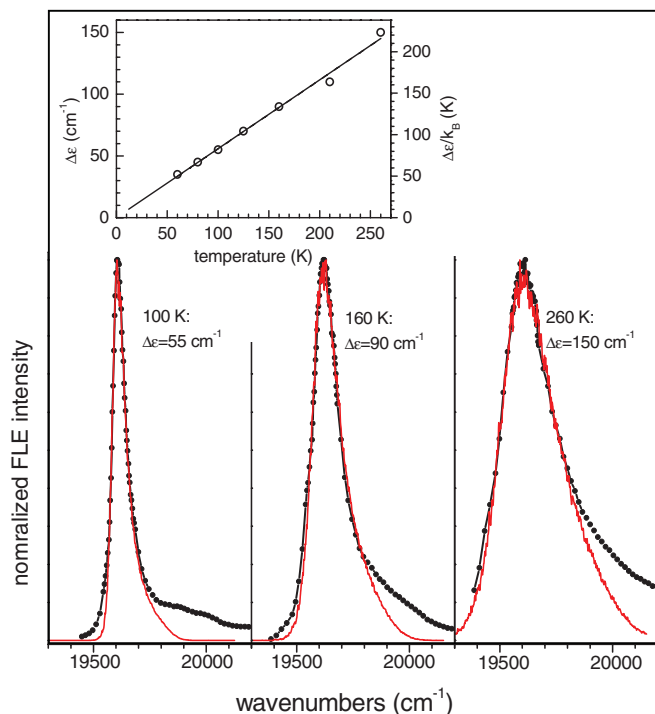


FIG. 7. Experimental (black) and calculated (red) fluorescence excitation spectra of the 0-0 line of the **BW** phase for a domain size ( $\tilde{N} \times \tilde{N}$ ) (red) with  $\tilde{N} = 7$  at three different temperatures ( $\lambda_{\text{det}} = 625$  nm (100 K), 160 K) and 548 nm (260 K)). The inset shows the temperature dependence of the parameter  $\Delta\varepsilon$ . Note the compressed scale of the wavenumber axis with respect to Fig. 5(a).

in the calculation described in Sec. III D 2) was neglected, too. Consequently, the thermal broadening estimated in this manner constitutes an upper limit.

We averaged a set of so calculated spectra and fitted the averaged spectra to the experimental spectra, for each temperature, by adjusting the parameter  $\Delta\varepsilon$ . Three exemplary FLE spectra are given in Fig. 7. In general we obtained good fits of the experimental line shapes. The deviation of the fits from the experimental spectra on the high energy side of the peaks is related to the contribution of unresolved low energetic vibronic modes on this side (cf. the spectrum in Fig. 2). Otherwise, the line shape is well described by the symmetric model function.

The resulting values for  $\Delta\varepsilon$  as a function of  $T$  (60–260 K) are also shown in the inset of Fig. 7. We find  $\Delta\varepsilon$  to increase linear with temperature and to be of the order of  $k_B T$ . We note that a linear dependence of the line width as a function of temperature and a Gaussian line shape due to scattering with phonons was also found in simulations of 2D J-aggregates by Schreiber and Toyozawa<sup>27</sup> taking only nearest neighbor interactions with identical couplings into account. Based on theoretical arguments, in Ref. 27 the disorder width  $\Delta\varepsilon$  was related to the temperature and it was claimed that  $\Delta\varepsilon \sim \sqrt{T}$ . This is in contrast to the experimental linear relationship found by us. We note that we also performed first more elaborate temperature dependent simulations of our spectra on the basis of the model described above using explicit phonon densities. Contrary to Ref. 27 these yielded also  $\Delta\varepsilon \sim T$  instead

of  $\Delta\varepsilon \sim \sqrt{T}$ . The reason for this difference is however unclear and will be subject to further work.

From an extrapolation of the experimentally determined values of  $\Delta\varepsilon(T)$  in Fig. 7 to 20 K, we estimate a contribution of the thermal broadening at 20 K of the order of  $10 \text{ cm}^{-1}$ . This width is compatible with the line width that we have observed for isolated molecules at well defined step sites at this temperature (i.e.,  $8 \text{ cm}^{-1}$ , see above), and it is significantly smaller than the FWHM of the BW phase at 20 K (i.e.,  $40 \text{ cm}^{-1}$ ). Given that the linear extrapolation of  $\Delta\varepsilon(T)$  still holds at low temperatures (20 K), we would indeed estimate an upper limit of  $10 \text{ cm}^{-1}$  for the thermal line broadening at 20 K, which would render it as small and leave the main contribution to the broadening to the finite size effect. However, so far we have not been able to extend our simulations to the range of low temperatures ( $<60$  K) in order to conjecture the true behavior of  $\Delta\varepsilon(T)$ . Such simulations have been performed, e.g., by Heijs *et al.*<sup>32</sup> and they demonstrate a power law behavior of  $\Delta\varepsilon(T)$  with some saturation at low  $T$ . Nevertheless these results cannot be easily transferred to our 2D system due to the differences in structure, size, dimensionality, and coupling constants. We hence plan to perform similar simulations on our systems for the future.

## IV. CONCLUSIONS

In conclusion we derive an understanding of the role of the finite size of molecular domains acting as J-aggregates on their optical spectra. The finite number of coupled molecules leads to several very close spaced transitions which are smeared out due to the statistical distribution of the domain size over some range. This leads to an asymmetric line profile of increased width. In the picture of an exciton band structure this can be understood as a weakening of the  $\Delta\mathbf{k} = 0$  rule by the finite size effect in combination with a non-zero dispersion of the exciton band. Thus the exciton states involved in an optical transition stem from a small region in  $\mathbf{k}$  space around the  $\Gamma$  point of the size  $k \leq 2\pi/L$  and exhibit slightly different energies  $E(\mathbf{k})$ . The energetic spread  $\Delta E$  of the contributing excitons, and hence the line width seen in the spectra, can be also estimated from the dispersion of exciton band structure at the  $\Gamma$  point (see Fig. 3) as  $\Delta E = \partial E/\partial \mathbf{k} \times (2\pi/L)$ . For the given domain size  $L = 100 \text{ \AA}$ , this yields  $\Delta E = 60 \text{ cm}^{-1}$  and  $27 \text{ cm}^{-1}$  for the  $\Gamma\text{M}$  and  $\Gamma\text{X}$  directions, respectively. Having in mind that for a more accurate estimation the different directions in  $\mathbf{k}$  space have to be averaged and different domain extensions in the respective directions have to be considered, these values for  $\Delta E$  are in very reasonable agreement with the experimentally observed FWHM of the 0-0 line of  $40 \text{ cm}^{-1}$ .

The observation of superradiance and the coherent coupling clearly proves that the excitons are truly delocalized states in our aggregates. It can be expected that the finite size broadening effect is the more pronounced the stronger the intermolecular coupling and hence the stronger the exciton dispersion is. Evidently, there is still room for much improvement of the model calculations on aggregates of finite size that were performed here. For instance, a correlation of the site-energy and the non-resonant interaction energy  $D_{\text{mol}}$  with

the position of the molecules within the domains could be included. In addition, coupling across domain boundaries and effects of specific domain size distributions could be of interest. Obviously a deliberate control of the domain size distribution from the experimental side, e.g., by using vicinal, stepped surfaces, or specific deposition parameters would be attractive.

## ACKNOWLEDGMENTS

Financial support by the DFG through the Research Unit 557 is gratefully acknowledged.

- <sup>1</sup>H. Fidder, J. Knoester, and D. A. Wiersma, *Chem. Phys. Lett.* **171**, 529 (1990).
- <sup>2</sup>E. O. Potma and D. A. Wiersma, *J. Chem. Phys.* **108**, 4894 (1998); H. Proehl, T. Dienel, R. Nitsche, and T. Fritz, *Phys. Rev. Lett.* **93**, 097403 (2004).
- <sup>3</sup>*Organic Electronics*, edited by H. Klauk (Wiley-VCH, Weinheim, 2006).
- <sup>4</sup>H. Marciniak, X. Q. Li, F. Würthner, and S. Lochbrunner, *J. Phys. Chem. A* **115**, 648 (2011); S. Valleau, S. K. Saikin, M. H. Yung, and A. A. Guzik, *J. Chem. Phys.* **137**, 034109 (2012).
- <sup>5</sup>*J-Aggregates*, edited by T. Kobayashi (World Scientific, Singapore, 1996).
- <sup>6</sup>A. Eisfeld and J. S. Briggs, *Chem. Phys.* **281**, 61 (2002).
- <sup>7</sup>D. P. Craig and S. H. Walmsley, *Excitons in Molecular Crystals* (Benjamin, New York, 1968).
- <sup>8</sup>S.-H. Lim, T. G. Bjorklund, F. C. Spano, and C. J. Bardeen, *Phys. Rev. Lett.* **92**, 107402 (2004); F. Meinardi, M. Cerminara, A. Sassella, R. Bonifacio, and R. Tubino, *Phys. Rev. Lett.* **91**, 247401 (2003); A. Camposo, M. Polo, S. Tavazzi, L. Silvestri, P. Spearman, R. Cingolani, and D. Pisignano, *Phys. Rev. B* **81**, 033306 (2010).
- <sup>9</sup>S. De Boer and D. A. Wiersma, *Chem. Phys. Lett.* **165**, 45 (1990).
- <sup>10</sup>D. H. Arias, K. W. Stone, S. M. Vlaming, B. J. Walker, M. G. Bawendi, R. J. Silbey, V. Bulović, and K. A. Nelson, *J. Phys. Chem. B* **117**(16), 4553 (2013).
- <sup>11</sup>M. Müller, J. Ikonov, and M. Sokolowski, *Surf. Sci.* **605**, 1090 (2011).
- <sup>12</sup>M. Müller, A. Langner, O. Krylova, E. Le Moal, and M. Sokolowski, *Appl. Phys. B: Lasers Opt.* **105**, 67 (2011).
- <sup>13</sup>M. Müller, A. Paulheim, C. Marquardt, and M. Sokolowski, *J. Chem. Phys.* **138**, 064703 (2013).
- <sup>14</sup>A. Paulheim, C. Marquardt, M. Müller, and M. Sokolowski, *Phys. Chem. Chem. Phys.* **15**, 4906 (2013).
- <sup>15</sup>M. Möbus, N. Karl, and T. Kobayashi, *J. Cryst. Growth* **116**, 495 (1992).
- <sup>16</sup>T. Dienel, C. Loppacher, S. C. B. Mannsfeld, R. Forker, and T. Fritz, *Adv. Mater.* **20**, 959 (2008).
- <sup>17</sup>E. Engel, K. Schmidt, D. Beljonne, J. L. Bredas, J. Assa, H. Frob, K. Leo, and M. Hoffmann, *Phys. Rev. B* **73**, 245216 (2006).
- <sup>18</sup>M. Wewer and F. Stienkemeier, *J. Chem. Phys.* **120**, 1239 (2004); M. Dvorak, M. Müller, T. Knoblauch, O. Bünermann, A. Rydlo, S. Minniberger, W. Harbich, and F. Stienkemeier, *J. Chem. Phys.* **137**, 164302 (2012).
- <sup>19</sup>M. Müller, A. Paulheim, C. Marquardt, and M. Sokolowski (unpublished).
- <sup>20</sup>J. Frenkel, *Phys. Rev.* **37**, 17 (1931).
- <sup>21</sup>A. S. Davydov, *Theory of Molecular Excitons* (Plenum, New York, 1971).
- <sup>22</sup>F. C. Spano, J. Clark, C. Silva, and R. H. Friend, *J. Chem. Phys.* **130**, 074904 (2009).
- <sup>23</sup>M. Hoffmann, K. Schmidt, T. Fritz, T. Hasche, V. M. Agranovich, and K. Leo, *Chem. Phys.* **258**, 73 (2000).
- <sup>24</sup>J. Roden, A. Eisfeld, M. Dvorak, O. Bünermann, and F. Stienkemeier, *J. Chem. Phys.* **134**, 054907 (2011); J. Bonça, S. A. Trugman, and I. Batisti, *Phys. Rev. B* **60**, 1633 (1999).
- <sup>25</sup>M. Müller, E. Le Moal, R. Scholz, and M. Sokolowski, *Phys. Rev. B* **83**, 241203(R) (2011).
- <sup>26</sup>W. P. Ambrose, T. Basche, and W. E. Moerner, *J. Chem. Phys.* **95**, 7150 (1991).
- <sup>27</sup>M. Schreiber and Y. Toyozawa, *J. Phys. Soc. Jpn.* **51**, 1528 (1982).
- <sup>28</sup>E. W. Knapp, *Chem. Phys.* **85**, 73 (1984); P. B. Walczak, A. Eisfeld, and J. S. Briggs, *J. Chem. Phys.* **128**, 044505 (2008).
- <sup>29</sup>H. Karacuban, S. Koch, M. Fendrich, T. Wagner, and R. Möller, *Nanotechnology* **22**, 295305 (2011).
- <sup>30</sup>F. C. Spano and H. Yamagata, *J. Phys. Chem. B* **115**, 5133 (2011).
- <sup>31</sup>F. C. Spano and S. Mukamel, *J. Chem. Phys.* **91**, 683 (1989).
- <sup>32</sup>D. J. Heijs, V. A. Malyshev, and J. Knoester, *J. Chem. Phys.* **123**, 144507 (2005).